Electronic Supplementary Material (ESI) for Soft Matter.

Electronic Supporting Information for:

Colloidal crystals of compliant microgel beads to study cell migration and mechanosensitivity in 3D

Katrin Wagner[1], Salvatore Girardo[1,2], Ruchi Goswami[1,2], Gonzalo Rosso[1,2,3], Elke Ulbricht[1], Paul Müller[1,2], Despina Soteriou[2], Nicole Träber[1,4], Jochen Guck[1,2]

[1]Center for Molecular and Cellular Bioengineering, Technische Universität Dresden, Tatzberg 47/49, 01307 Dresden, Germany

[2]Max-Planck-Institut für die Physik des Lichts & Max-Planck-Zentrum für Physik und Medizin, Staudtstr. 2, 91058 Erlangen

[3]Institute of Physiology II, University of Münster, Münster, Germany

[4]Leibniz-Institut für Polymerforschung Dresden e. V., Hohe Str. 6, 01069 Dresden, Germany

Theoretical oxygen supply

An important parameter to consider in 3D cultures is the oxygen supply, since limitations in oxygen can influence cellular behavior such as survival, proliferation and migration [1,2]. Computational simulations were used to calculate the amount of oxygen in the 3D colloidal crystals in the ibidi µ-Slide VI$^{0.4}$. The µ-slide has a gas-permeable ibidi polymer coverslip bottom (ibidi GmbH), which allows diffusion of O_2 and CO_2 into the cell culture channel. The diffusion of gas into the colloidal crystal through the µ-slide bottom is described by the following equations:

$$\frac{\partial c_i}{\partial t} + \nabla \cdot (-D_i \nabla c_i) = R_i \quad (1)$$

$$N_{O,C} = P \cdot \left(p_g - \frac{c}{X_{O2}}\right) \quad (2)$$

$$R_i = -\frac{1}{Y_{X/O2}} \cdot \mu \cdot C_x(t) \quad (3)$$

$$\mu = \mu_{max} \cdot \frac{C_s}{K_{mS}+C_s} \cdot \frac{C_{O2}}{K_{mO}+C_{O2}} = \mu_{max} \cdot \frac{C_{O2}}{K_{mO}+C_{O2}} \quad (4)$$

$$C_x(t) = \frac{n_{cell}}{A \cdot H_1} \cdot \exp\left(\mu_{max} \cdot \frac{C_{O2}}{K_{mO}+C_{O2}} \cdot t\right) \quad (5)$$

$$R_i = -OCR \cdot \frac{C_{O2}}{K_{mO}+C_{O2}} \cdot \frac{n_{cell}}{A \cdot H1} \cdot \exp\left(\mu_{max} \cdot \frac{C_{O2}}{K_{mO}+C_{O2}} \cdot t\right) \quad (6)$$

where $\dot{N_{o,c}}$ is the inward flux of oxygen through the plastic bottom, $\dot{R_\iota}$, an oxygen consumption rate (including cell proliferation). A simple Monod kinetic with substrate inhibition was chosen for cell proliferation (equ. (3), (4)), where oxygen was assumed to be the only limiting substrate [3,4]. μ_{max} was defined as the maximal cell growth rate, $C_x(t)$ as cell growth by proliferation and $Y_{X/O2}$ the yield of cells per unit oxygen which was related to the oxygen consumption rate (OCR) per cell ($\frac{1}{Y_{X/O2}} = OCR$). Implementing the doubling time of 20 h for NIH3T3 fibroblasts into equ. (5), a maximal growth rate $\mu_{max} = 9.627 \cdot 10^{-6}\, s^{-1}$ was determined. Other parameters used for simulations are defined in Table 1. We used COMSOL Multiphysics 5.2 to estimate whether oxygen gradients were generated in our colloidal crystals by changing the diffusion coefficient, D, and cell concentration, n_{cell} (Figure 2B-D). To confirm a correct model implementation a diffusion coefficient four times smaller than the diffusion coefficient at 37°C ($D << D_{O2}$) was used that established an oxygen concentration gradient over the channel height and over time (Figure 2B). The gradients were caused by inhibited oxygen diffusion through the bottom of the channel and slow diffusion through the channel volume to replace the oxygen consumed by cells. When implementing D_{O2} for oxygen in medium at 37°C [5] and 20,000 cells heterogeneously distributed in the channel volume, an oxygen gradient over time was established (Figure 2C). Oxygen concentration reached 0.078 mol/m³ after 27 h, which was still above reported hypoxic conditions (~ 0.02 mol/m³ [6]). This result suggested that a sufficient oxygen gradient can be established in our scaffolds. By decreasing the cell amount to 10,000 cells per channel, the established oxygen concentration gradient was even smaller (Figure 2D), which was expected with a correct model implementation.

Table 1: Parameters for oxygen simulation performed in COMSOL Multiphysics 5.2

Parameter	Value	Unit	Definition

D_{O2}	$2.69*10^{-9}$	[m^2/s]	Oxygen diffusion coefficient in medium at 37°C [5]
OCR	$1.19*10^{-17}$	[mol/(s)]	Oxygen consumption rate (OCR) per fibroblast [7]
n_{cell}	10,000 20,000		Cell number
A	38	[mm^2]	Considered area of channel bottom
H_1	400	[µm]	Liquid height (i.e. channel height)
P	$1.1193*10^{-7}$	[$mol/(m^2*s*bar)$]	Permeability at 23°C (personal communication with ibidi GmbH)
H_2	170	[µm]	Membrane thickness
X_{O2}	1.053	[$mol/(m^3*bar)$]	Mole fraction solubility
p_g	0.21	[bar]	Ambient partial pressure of oxygen
K_{mO}	$1.0*10^{-3}$	[mol/m^3]	Michaelis-Menten Constant for Oxygen [8]
B	3.8	[mm]	Channel width
D_{small}	$2.69*10^{-13}$	[m^2/s]	Small diffusion coefficient
D_2	$1.6*10^{-9}$	[m^2/s]	Reduced oxygen diffusion coefficient for hydrogels [9]

Considering the established gradients, cellular function should be conserved even at lower oxygen concentrations for cell culture experiments lasting at least 24 h. Taken together, modeling the diffusion in the colloidal crystal suggested that cells should theoretically be able to survive and proliferate in the 3D scaffolds.

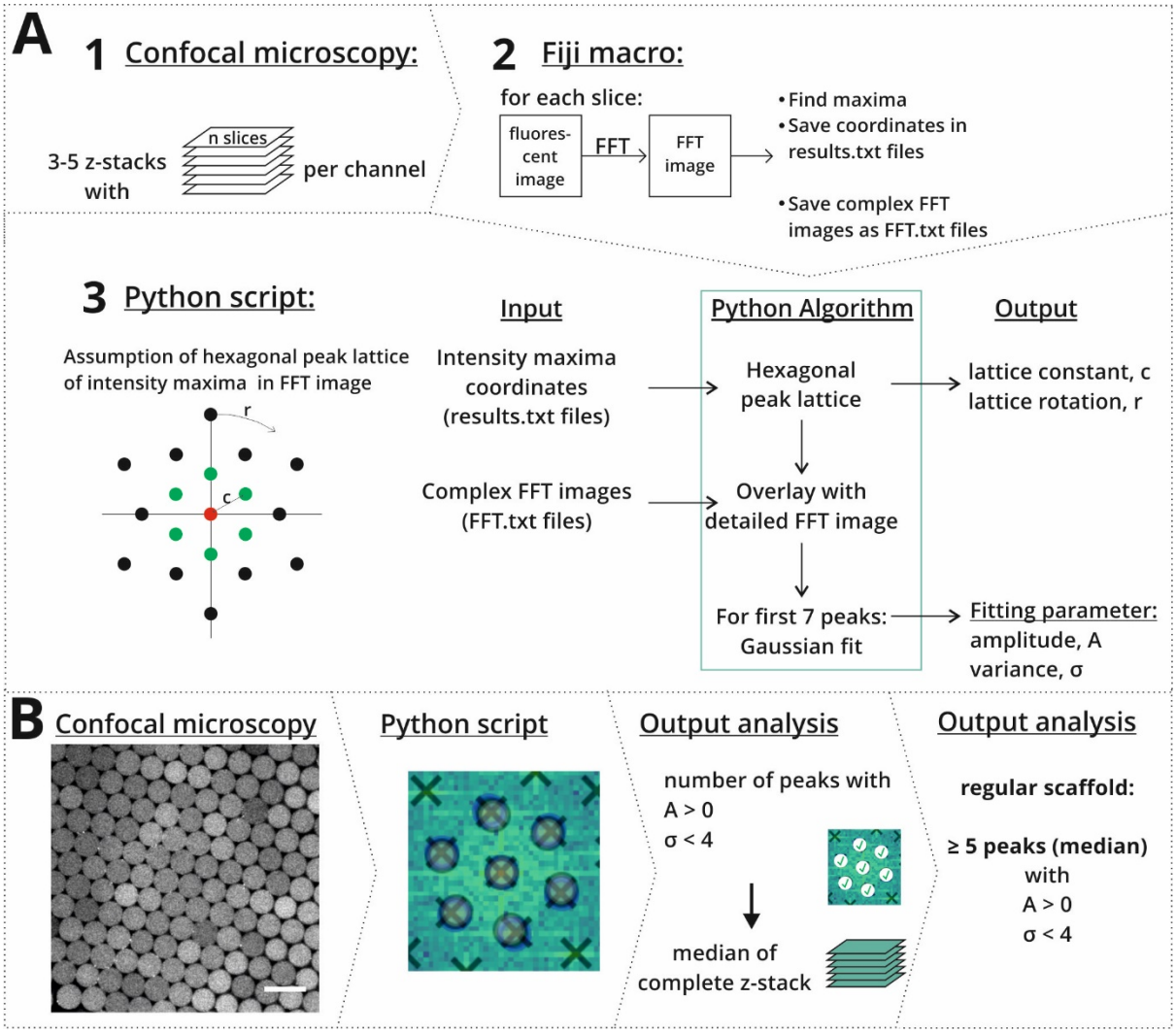

SI Figure 1: Characterization of 3D microgel bead colloidal crystal regularity. A) Image processing work flow. B) Exemplary image processing and output data analysis work flow for regular 3D microgel bead colloidal crystals. At least three randomly chosen positions per colloidal crystal were imaged by fluorescence confocal microscopy (A-1, B). For each slice of the acquired 3D-stacks, a Fast Fourier Transformation (FFT) was performed as regularity patterns can be easily recognized in Fourier space. A custom-written macro in FIJI determined the intensity maxima in Fourier space and saved the coordinates as well as the complex FFT images (A-2). A custom-written Python script determined a hexagonal peak lattice based on the intensity maxima and overlaid this peak lattice with the FFT images (A-3, B). The center peak is red; the main regularity peaks are green. For the first seven intensity peaks a Gaussian fit was performed as these peaks describe the main regularity of the real image. The output data were the amplitude, A, and the variance, σ, of the Gaussian fits for each peak and the number of peak fits with $A > 0$ and $\sigma < 4$. This was performed for every slice of the acquired z-stacks and the median number of peak fits that fulfilled these requirements was determined (see Figure 1E).

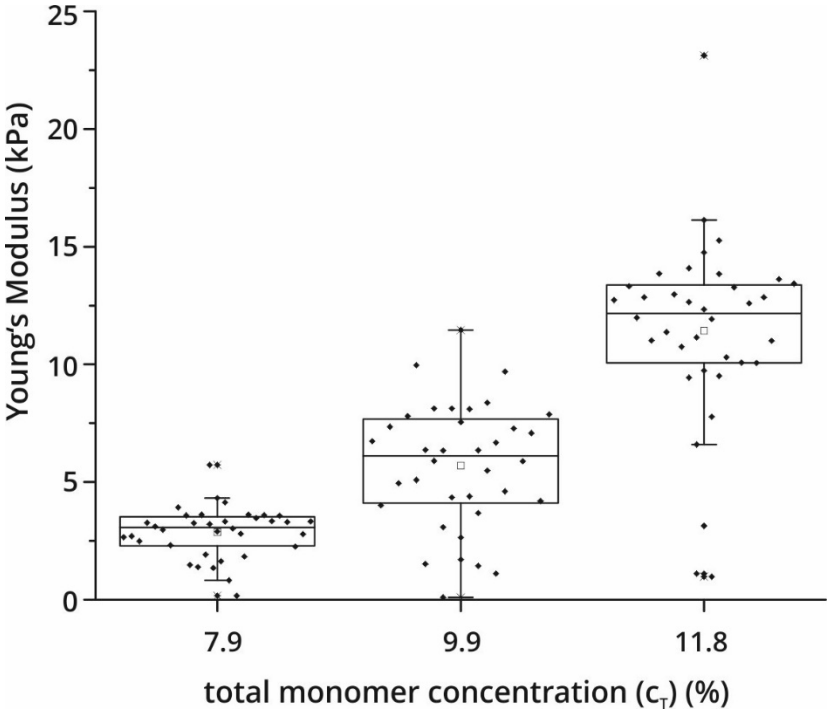

SI Figure 2: Young's moduli of different PAAm microgel bead batches (varied total monomer concentration c_T) functionalized with Cy5-tagged Poly-L-Lysine (1.34 pg/bead). Young's modulus was determined by AFM nanoindentation (n = 36 for each composition).

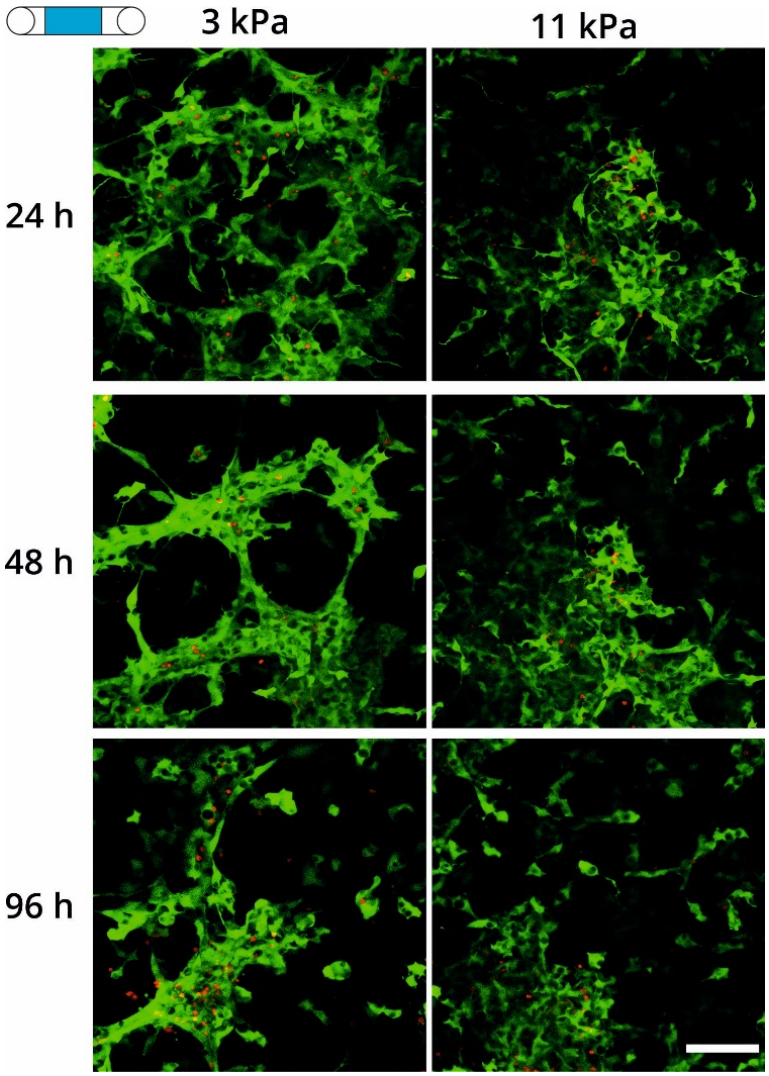

SI Figure 3: Representative confocal images of fibroblasts randomly seeded in colloidal crystals with beads having a mean Young's modulus of 3 kPa or 11 kPa over 96 h. PAAm microgel beads had a total monomer concentration (c_T) of 7.9% and 11.8%, respectively, and were coated with Poly-L-Lysine-Cy5. Medium was replaced daily and supplemented with propidium iodide (PI) to monitor cell death. Images show maximum projections. Green: fibroblasts; red: nuclei of dead cells (PI). Scale bar: 100 µm.

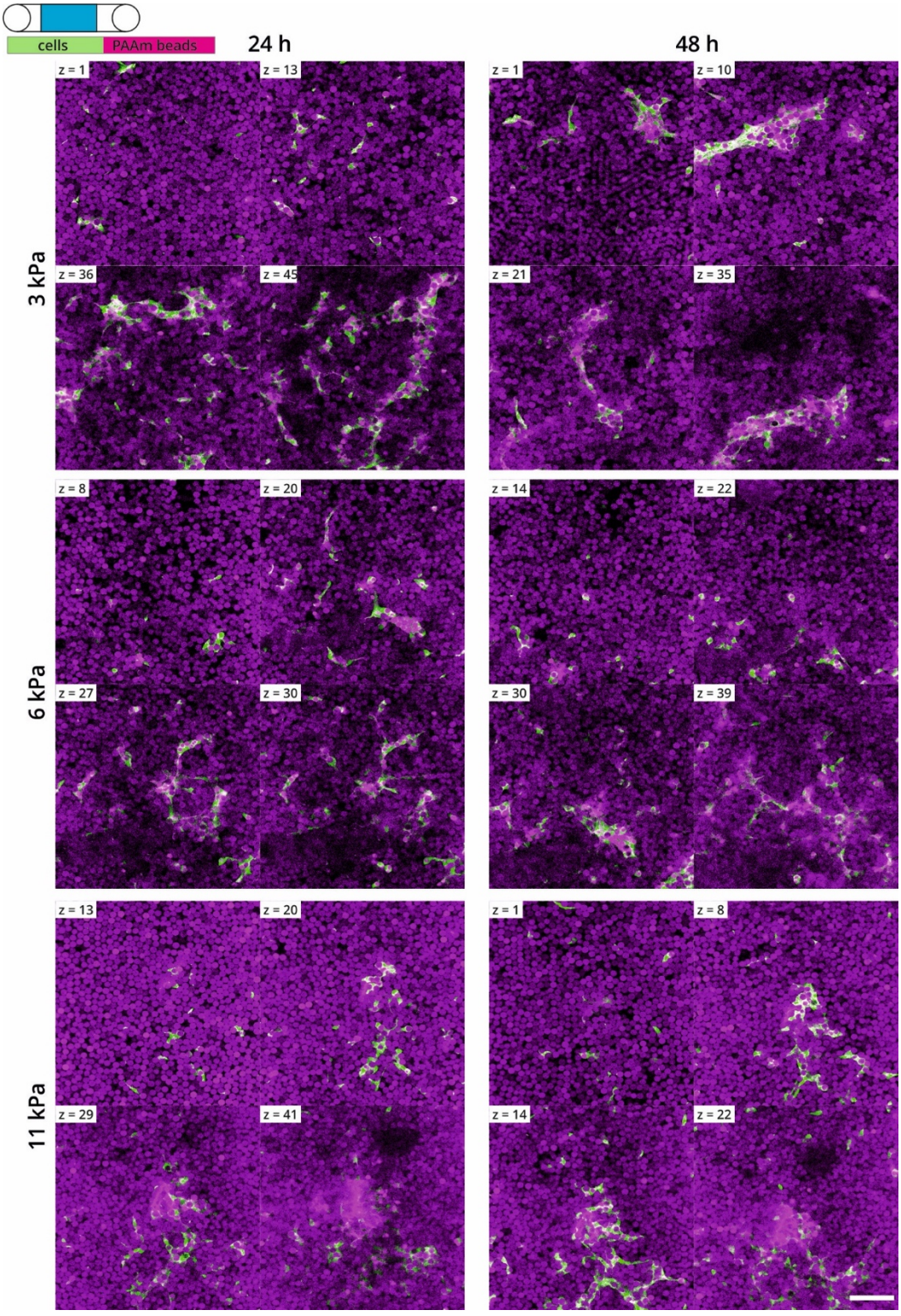

SI Figure 4: Representative confocal images of NIH3T3/GFP fibroblasts (green) in 3D microgel bead colloidal crystals with different stiffness over 48 h. Polyacrylamide (PAAm) microgel beads were functionalized with PLL-Cy5 (magenta). Images show single z-slices (z-position is indicated in upper left corner of each image). The average Young's modulus of respective PAAm bead batches was determined by AFM nanoindentation. 20,000 cells were randomly seeded in each channel. Scale bar: 100 µm.

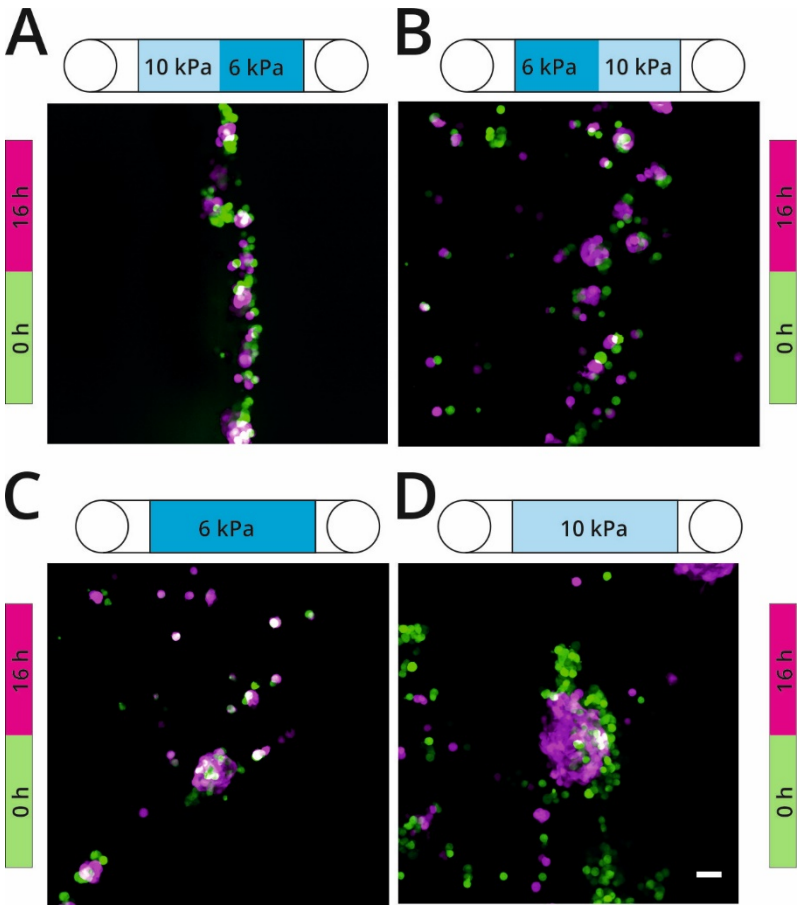

SI Figure 5: NIH3T3/GFP fibroblasts migrating through non-functionalized colloidal crystals overnight. Overlay of maximum projections of fibroblast fluorescence signal with green as starting point (t = 0 h) and magenta as end point (t = 16 h). A, B) Colloidal crystal step stiffness. C, D) Homogeneous colloidal crystal stiffness. 10,000 cells were seeded. Images were acquired with a spinning disk microscope (Andor Dragonfly). Scale bar: 50 µm.

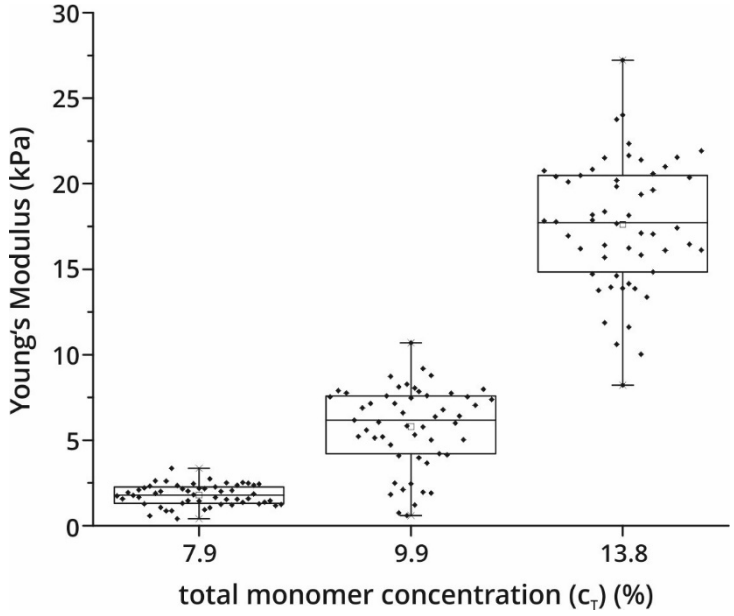

SI Figure 6: Young's moduli of different PAAm microgel bead batches (varied total monomer concentration c_T) functionalized with Poly-D-Lysine and laminin. Young's modulus was determined by AFM nanoindentation (n = 52 for each composition).

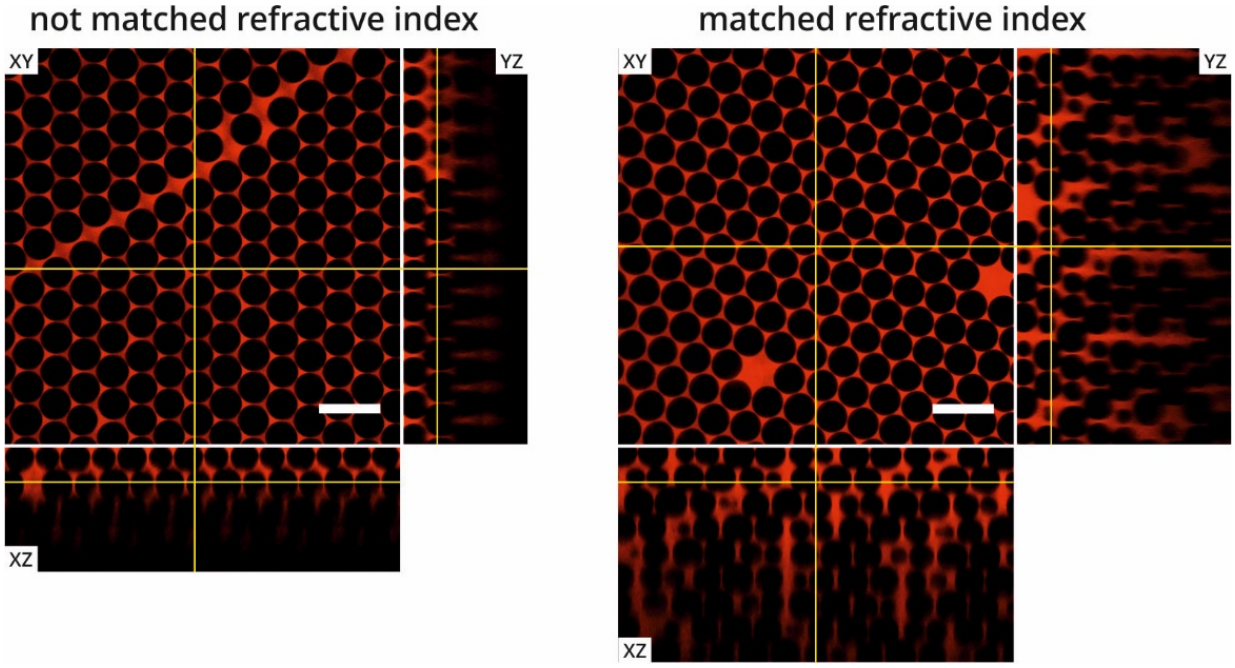

SI Figure 7: Orthogonal view of PMMA colloidal crystals without refractive index matching and with refractive index matching. PMMA beads are black and the interstitial space is filled with Rhodamine-6G and 2,2-thiodiethanol. Scale bars: 100 µm.

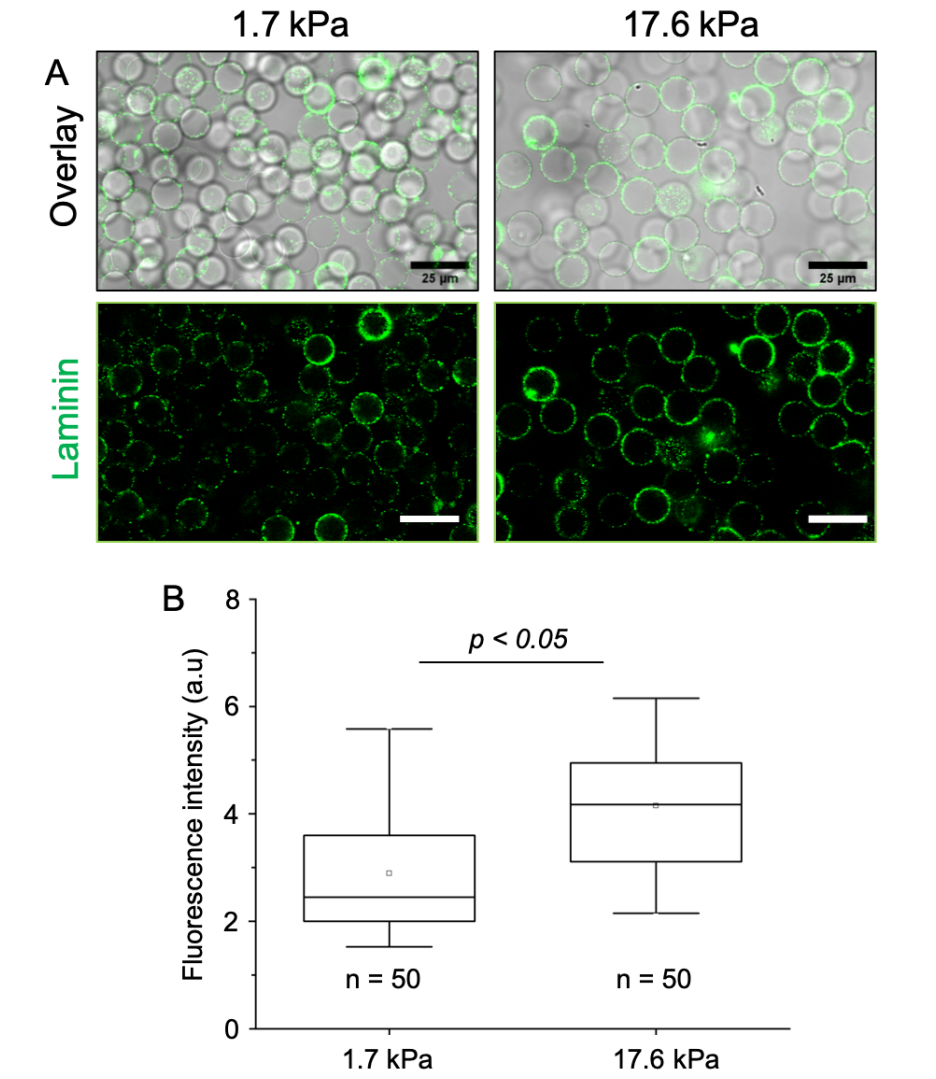

114

115

116 SI Figure 8: Quantification of laminin binding on PAAm beads of different stiffness.
117 Fluorescence images in A show the laminin staining (green) on soft (left images) and stiff
118 (right images) PAAm beads. Graph in B shows the fluorescence quantification of laminin
119 binding. Statistical differences were analysed with Mann-Whitney test.

120

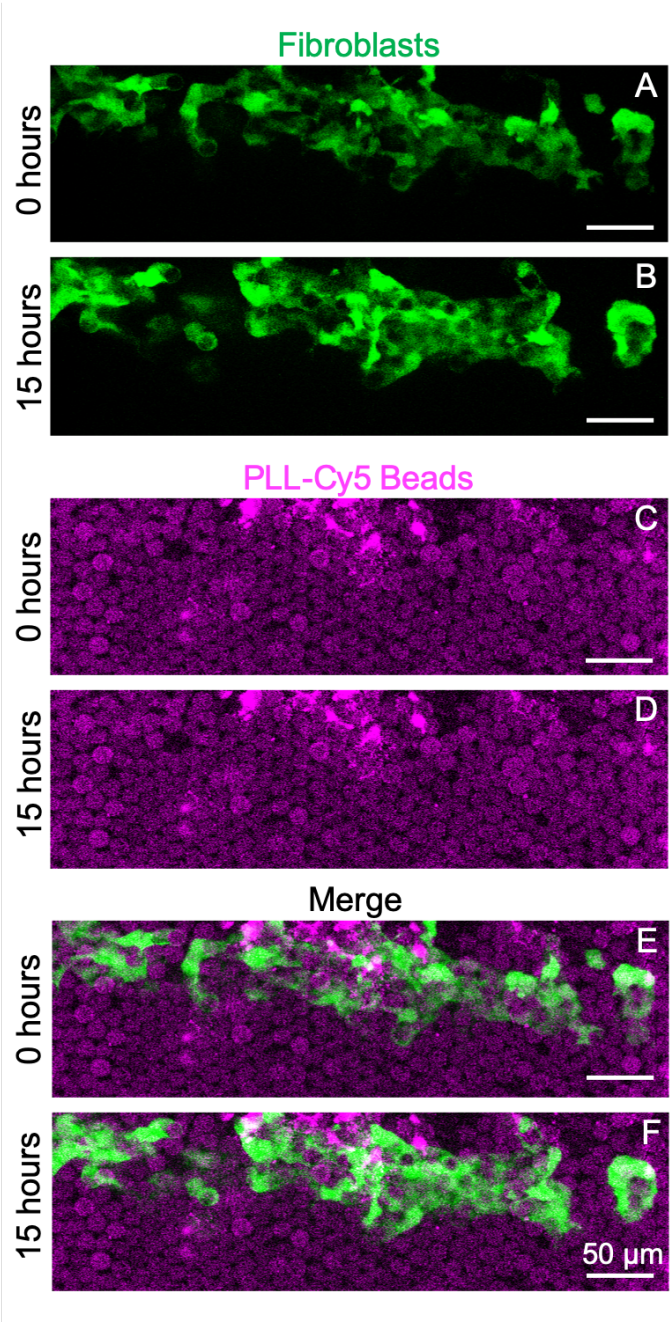

SI Figure 9: Embedding and migration of fluorescently labelled cells in well-organized PAAm-bead scaffold. PLL-coated beads in magenta; fibroblasts in green. Top and bottom panels show different time points during the experiment: time 0h and 15h respectively. A and B are representative images of fibroblasts embedded in microgel beads scaffolds, shown separately in C and D. Merged images of fibroblasts and beads are shown in panels E and F.

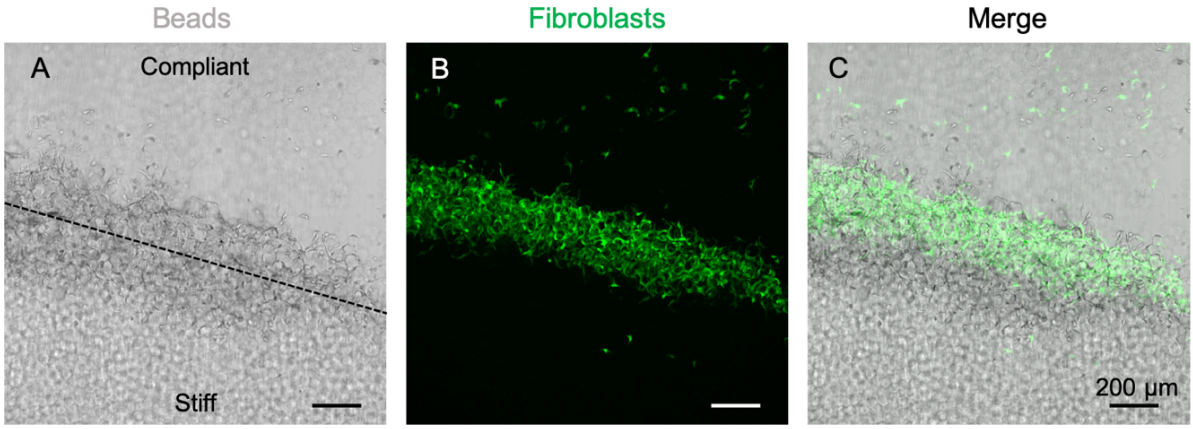

SI Figure 10: Using transmission light microscopy used to precisely define the interface zone between stiff and compliant microbeads. Representative bright field image in A shows the interface zone (dashed line) between compliant (top) and stiff (bottom) PAAm beads. Image in B shows GFP-labelled fibroblasts (green) embedded in the 3D scaffold. C merged image of fibroblasts and beads.

Bibliographic references

1 W. G. Taylor, R. F. Camalier and K. K. Sanford, *J. Cell. Physiol.*, 1978, **95**, 33–40.

2 M. Csete, *Ann. N. Y. Acad. Sci.*, 2005, **1049**, 1–8.

3 J. Monod, *Annu. Rev. Microbiol.*, 1949, **3**, 371–394.

4 T. I. Croll, S. Gentz, K. Mueller, M. Davidson, A. J. O'Connor, G. W. Stevens and J. J. Cooper-White, *Chem. Eng. Sci.*, 2005, **60**, 4924–4934.

5 A. Richter, K. K. Sanford and V. J. Evans, *JNCI J. Natl. Cancer Inst.*, 1972, **49**, 1705–1712.

6 N. Korin, A. Bransky, U. Dinnar and S. Levenberg, *Lab Chip*, 2007, **7**, 611.

7 I. Streeter and U. Cheema, *Analyst*, 2011, **136**, 4013.

8 B. A. Wagner, S. Venkataraman and G. R. Buettner, *Free Radic. Biol. Med.*, 2011, **51**, 700–712.

9 A. C. Hulst, H. J. H. Hens, R. M. Buitelaar and J. Tramper, *Biotechnol. Tech.*, 1989, **3**, 199–204.